Supporting information

Thiophene-doped resorcinol-formaldehyde resin photocatalyst for efficient H_2O_2 production via enhanced selectivity toward two-electron ORR pathway

Yuxin Min, [a] Yunjie Luo, [a] Yanan Tian, [a] Xuefei Wang, *[a] Ping Wang, [a] Feng Chen [a] and Huogen Yu *[b]

[a] School of Chemistry, Chemical Engineering and Life Sciences, Wuhan University of Technology, Wuhan 430070, PR China

[b] Laboratory of Solar Fuel, Faculty of Materials Science and Chemistry, China University of Geosciences, Wuhan 430074, PR China

* Corresponding authors

E-mail: xuefei@whut.edu.cn (X. Wang); yuhuogen@cug.edu.cn (H. Yu)

Experimental section

Characterizations

The morphology and microstructure of the photocatalysts were analyzed by field emission scanning electron microscopy (SEM, JSM-7500F, Japan) and high-resolution transmission electron microscopy (HRTEM, Talos F200S, Thermo Fisher). The crystal structures of the photocatalysts were obtained using an X-ray diffractometer (XRD, Rigaku Ultima III, Japan) with Cu Kα radiation. Fourier transform infrared (FT-IR) spectra were recorded using a Fourier transform infrared spectrometer (Nicolet6700, Thermo Fisher Scientific, USA). The ultraviolet-visible (UV-vis) absorption spectra were obtained using a UV-2450 instrument (Shimadzu, Japan, $BaSO_4$ as the reference sample) to characterize the optical absorption properties. The ^{13}C nuclear magnetic resonances (^{13}C-NMR) spectra were obtained by using a solid-state nuclear magnetic resonance spectrometer (AVANCE III, Bruker, Germany). The surface chemical states of the different elements of the various samples were gained using an X-ray photoelectron spectrometer (XPS, Thermo KRATOA XSAM800) and radiation from an Al Kα source. The XPS spectra were acquired by a Thermo Scientific K-Alpha instrument with Al Kα X-ray radiation. The binding energies of XPS for all elements were calibrated with amorphous carbon peaks of 284.6 eV. The time-resolved photoluminescence (TRPL) spectra were recorded using the FLS1000 transient fluorescence spectrometer (Edinburgh Instruments, UK).

Photocatalytic H_2O_2 production test

In brief, 50 mg of photocatalyst was fully dispersed in 50 mL of pure water. Oxygen was continuously supplied to the system until the solution achieved oxygen saturation. Next, the photocatalytic reactor was irradiated by an LED lamp (λ = 420 nm) with a light intensity of 12.5 mW cm^{-2}. Take 2 mL reaction solution every 30 min, and filter through a water-based disposable needle filter to remove the photocatalyst to obtain the supernatant solution, and then 2 mL potassium titanium oxalate solution (0.02 mol L^{-1}) was added for color reaction. The H_2O_2 concentration was obtained by detecting the absorbance of the solution using a UV visible spectrophotometer (UV-1000, Japan).

Photocatalytic H_2O_2 decomposition test

50 mg of photocatalyst and 50 mL of deionized water were added to the photocatalytic reaction flask, and then 25 μL of H_2O_2 solution (30%) was added to it with a pipette gun, and N_2 was passed through and bubbled for 30 min to remove dissolved oxygen. Samples were taken every 30 min and the H_2O_2 concentration was measured in the same way.

Cycling test of photocatalysts

During the first cycle test, the T_5RF_{95} (50 mg) photocatalyst and pure water (50 mL) were added into the photocatalytic reaction bottle, and the H_2O_2 concentration was

detected by the same method after the photocatalytic reaction for each 30 min. Then, the reacted suspension was filtered, washed, and dried for photocatalyst recovery. The same steps were used for the subsequent five-cycle tests.

The AQY calculation

The apparent quantum yield (AQY) is one of the important indicators for evaluating the efficiency of the H_2O_2 photocatalytic production. The AQY parameter was calculated via the following formula[1]:

$$AQY = \frac{2M_{H_2O_2}N_A hc}{EAt\lambda} \times 100\%$$

$$= 6.65 \times 10^{-5} \times \frac{M_{H_2O_2}}{EA\lambda} \times 100\% \quad \text{(S1)}$$

where photocatalytic reaction irradiation time t (s), Avogadro constant N_A (mol^{-1}), Planck constant h (J•s), and light velocity c ($m\ s^{-1}$) are all constants with values of 3600, 6.022×10^{23}, 6.626×10^{-34}, and 3.0×10^{8}, respectively. Furthermore, $M_{H_2O_2}$ represents the molar amount of H_2O_2 produced by the average reaction for 1 h (7.55×10^{-6} mol), E represents the intensity of the irradiated light (12.5 mW cm^{-2}), A represents the area of light radiation (3.14 cm^2), λ represents the wavelength of the incident monochromatic light (420 nm). Hence, the AQY of T_5RF_{95} photocatalyst with optimal photocatalytic performance in this work can be calculated as:

$$AQY = \frac{(6.65 \times 10^{-5} \times 7.55 \times 10^{-6})}{(12.5 \times 10^{-3} \times 3.14 \times 420 \times 10^{-9})} \times 100\%$$

$$= 3.04\%$$

Photoelectrochemical measurements

The electrochemical measurements including photoelectric current, electrochemical impedance spectroscopy (EIS), Mott-Schottky curve, the linear scanning voltammetry (LSV) curves, and the response of the instantaneous photocurrent with time were measured on CHI760E electrochemical workstation. The Pt sheet and Ag/AgCl electrode were used as the counter and reference electrode, respectively. All photoelectrochemical tests were carried out under the condition of Na_2SO_4 solution (0.5 mol L^{-1}, pH = 7) as electrolyte. The working electrodes were prepared on an FTO substrate with an active area of about 1.0 cm.[2]

The working electrode was prepared in detail as follows: firstly, the FTO conductive glass is washed successively with acetone, ethanol, and deionized water. Secondly, the prepared photocatalytic samples (10 mg) were dissolved into anhydrous ethanol (2.5 mL), and the suspension was ultrasonic-treated for 30 min. Dilute 5 wt% D-520 Nafion suspension solution (1 mL) to 1 wt% with anhydrous ethanol (4 mL). Finally, 0.5 mL diluted D-520 Nafion solution was mixed with 0.5 mL of the photocatalyst-ethanol solution prepared above, and ultrasonic treatment was performed for 30 min. The 300 μL suspension was uniformly coated on the FTO conductive glass in batches and dried at 65 ^{o}C for 12 h. The effective film area coated on FTO conductive glass is 1 × 1 cm^2. The potential *vs.* Ag/AgCl reference electrode was converted to the potential relative to the normal hydrogen electrode (*vs.* NHE) according to the Nernst equation:

$$E(vs.\,NHE) = E(Ag/AgCl) + 0.197\,V \quad \text{(S2)}$$

Rotating disk electrode (RDE) test

The electron transfer number (n) of ORR was analyzed by linear sweep voltammetry (LSV) on the RDE in phosphate buffered saline (PBS) solution (0.1 M, pH = 7) under oxygen purged condition. The Pt wire electrode and Ag/AgCl electrode were used as the counter and reference electrode, respectively. 50 mg catalysts and 50 μL Nafion were dispersed in 2 mL EtOH solution by sonication for 30 min, then a slurry was obtained. And 20 μL of the slurry was placed onto the glace carbon disk and dried naturally. The scan rate was set to 10 mV s^{-1}, and the rotating speed was set as 400-2025 rpm. The n was obtained by the Koutecky-Levich equation:

$$j^{-1} = j_k{}^{-1} + B^{-1}\omega^{-1/2} \quad \text{(S3)}$$

$$B = 0.2nFv^{-1/6}CD^{2/3} \quad \text{(S4)}$$

where j is the current density, j_k is the kinetic current density, ω is the rotating speed (rpm), F is the Faraday constant (96485 C mol^{-1}), v is the kinetic viscosity of water (0.01 $cm^2\ s^{-1}$), C is the bulk concentration of O_2 in the water (1.26×10^{-6} mol cm^{-3}), and D is the diffusion coefficient of O_2 (2.75×10^{-5} $cm^2\ s^{-1}$), respectively.

Rotating ring disk electrode (RRDE) test

The Pt wire electrode and Ag/AgCl electrode were used as the counter and reference electrode, respectively. The working electrode on RRDE was prepared via the same method as the RDE test. The RRDE test was conducted in PBS solution (0.1 M, pH =

7) under N_2 atmosphere with the scan rate of 10 mV s^{-1} and a rotation speed of 1600 rpm. The potential of the ring electrode was set to 0.6 V (*vs.* Ag/AgCl) to detect H_2O_2. The electron transfer number (n) was determined by the following equation[3]:

$$n = 4 \times \frac{I_d}{I_d + I_r/N} \quad \text{(S5)}$$

where I_d was disk current, I_r was ring current, and N was the current collection efficiency (N) of the Pt ring. N was determined to be 0.38 from the reaction of reduction of $K_3Fe[CN]_6/K_2Fe[CN]_6$.

DFT calculation

The density functional theory (DFT) calculations were performed via the Gaussian 16 suite of programs. The structures of the molecules of RF and TRF were fully optimized at the B3LYP-D3BJ/6-311G(d) level of theory[2, 4]. The molecular orbital levels of RF and TRF resins, including the highest occupied molecular orbital (HOMO) and the lowest unoccupied molecular orbital (LUMO) were investigated via theoretical calculations. The hole-electron analysis was carried out on the Multiwfn software based on the TD-B3LYP/6-311G(d)[5, 6]. The adsorption energy (E_{ads}) of the O_2 molecule on the photocatalyst can be defined as:

$$E_{ads} = E_{total} - E_{slab} - E_{O_2} \quad \text{(S6)}$$

where E_{total}, E_{slab}, and E_{O_2} are the total energy after the adsorption of O_2 on the surface of the photocatalytic catalyst, the energy of the original photocatalyst, and the energy of the O_2 molecule under vacuum, respectively. Several O_2 adsorption models of resins

were fully considered in the DFT calculation, and the most stable adsorption mode was determined according to the adsorption energy. By definition, the stronger the adsorption of molecules on the phenolic resin catalyst surface, the more negative the value of the adsorption energy.

Supporting Figures

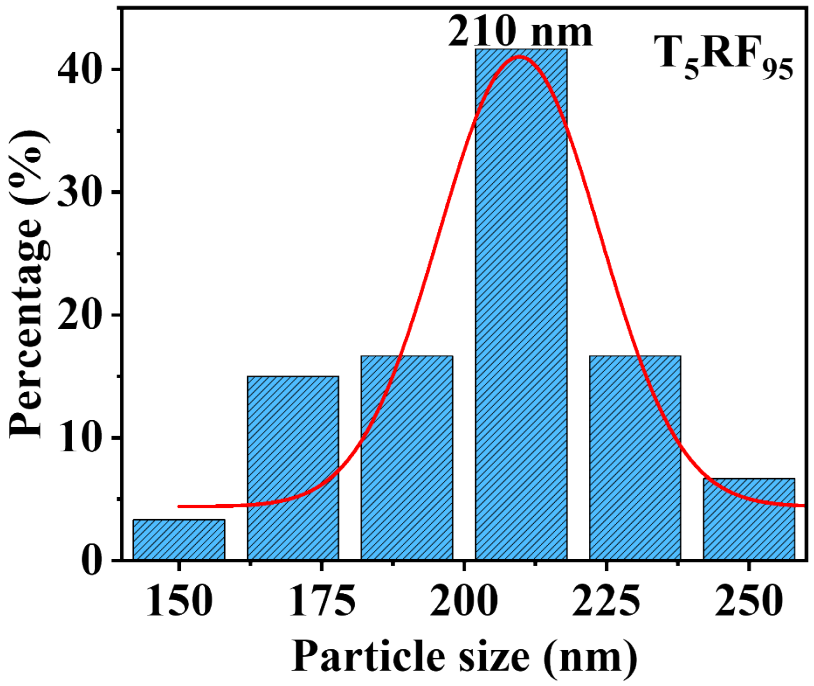

Fig. S1. Particle size distribution diagram of the T_5RF_{95} sample.

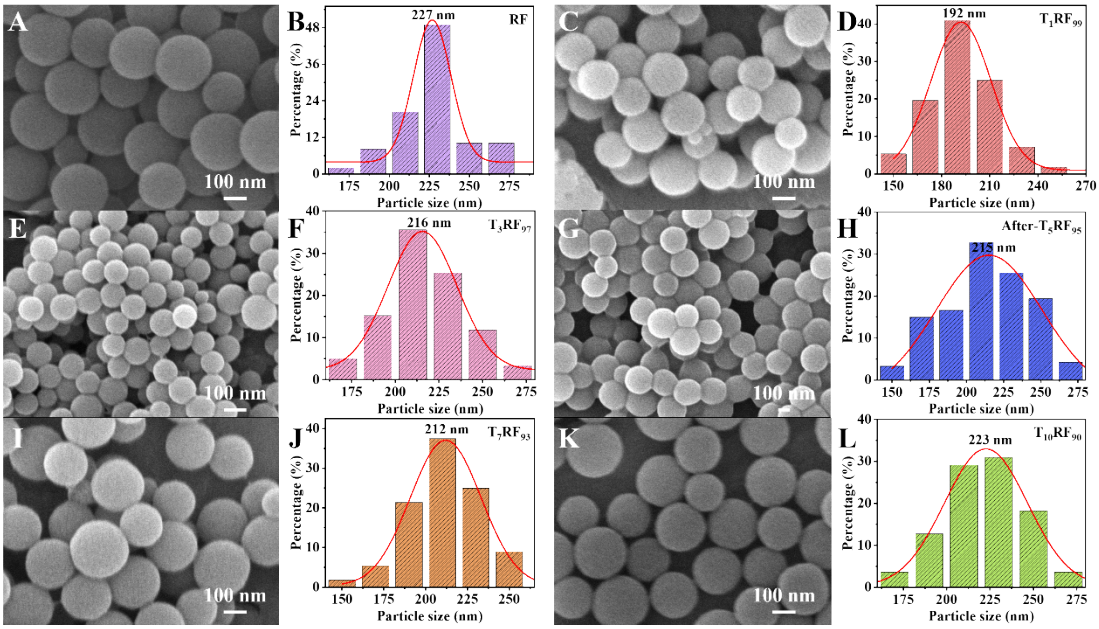

Fig. S2. SEM images and particle size distribution diagrams of various samples: (A-B) RF, (C-D) T_1RF_{99}, (E-F) T_3RF_{97}, (G-H) T_5RF_{95} after photoreaction, (I-J) T_7RF_{93}, and (K-L) $T_{10}RF_{90}$.

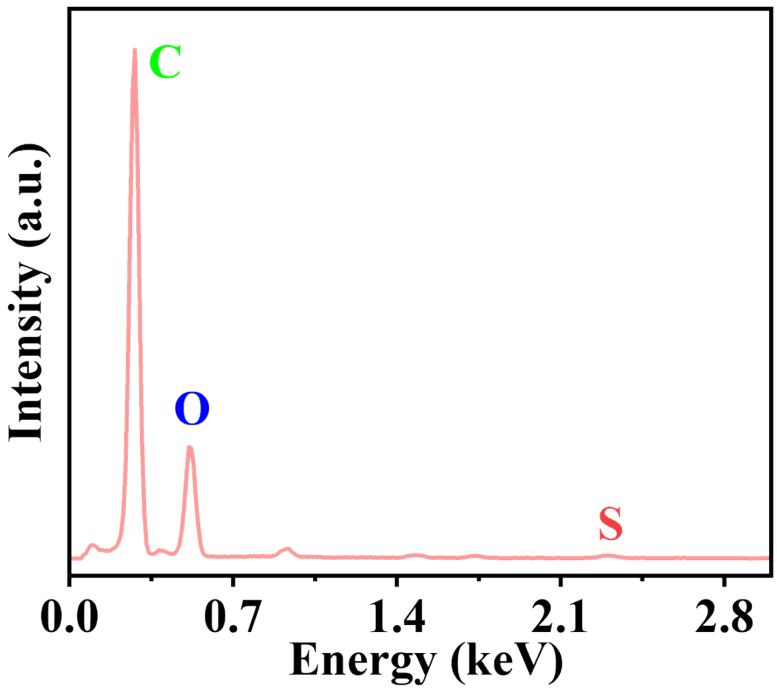

Fig. S3. EDX spectrum of the T_5RF_{95} photocatalyst.

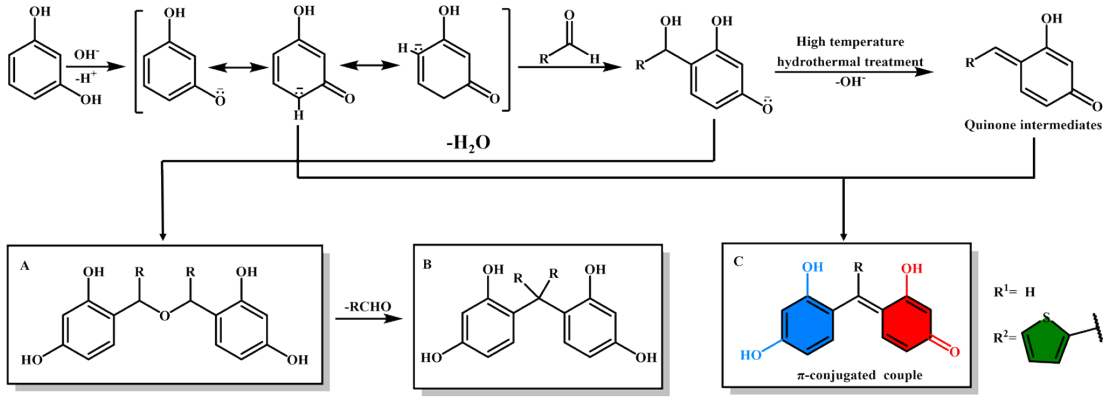

Fig. S4. Mechanism of reaction and structural schematic diagrams.

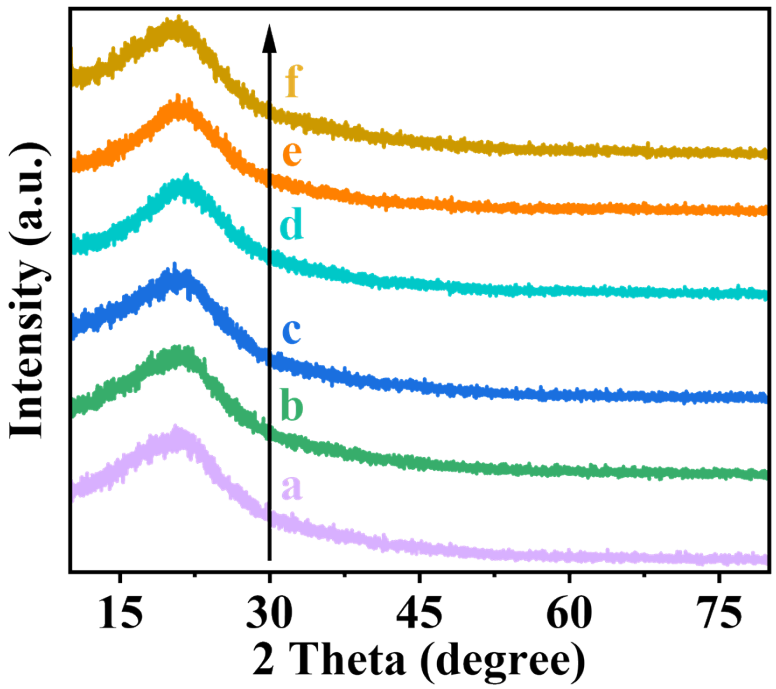

Fig. S5. X-ray diffraction (XRD) patterns of various resins: (a) RF, (b) T_1RF_{99}, (c) T_3RF_{97}, (d) T_5RF_{95}, (e) T_7RF_{93}, and (f) $T_{10}RF_{90}$.

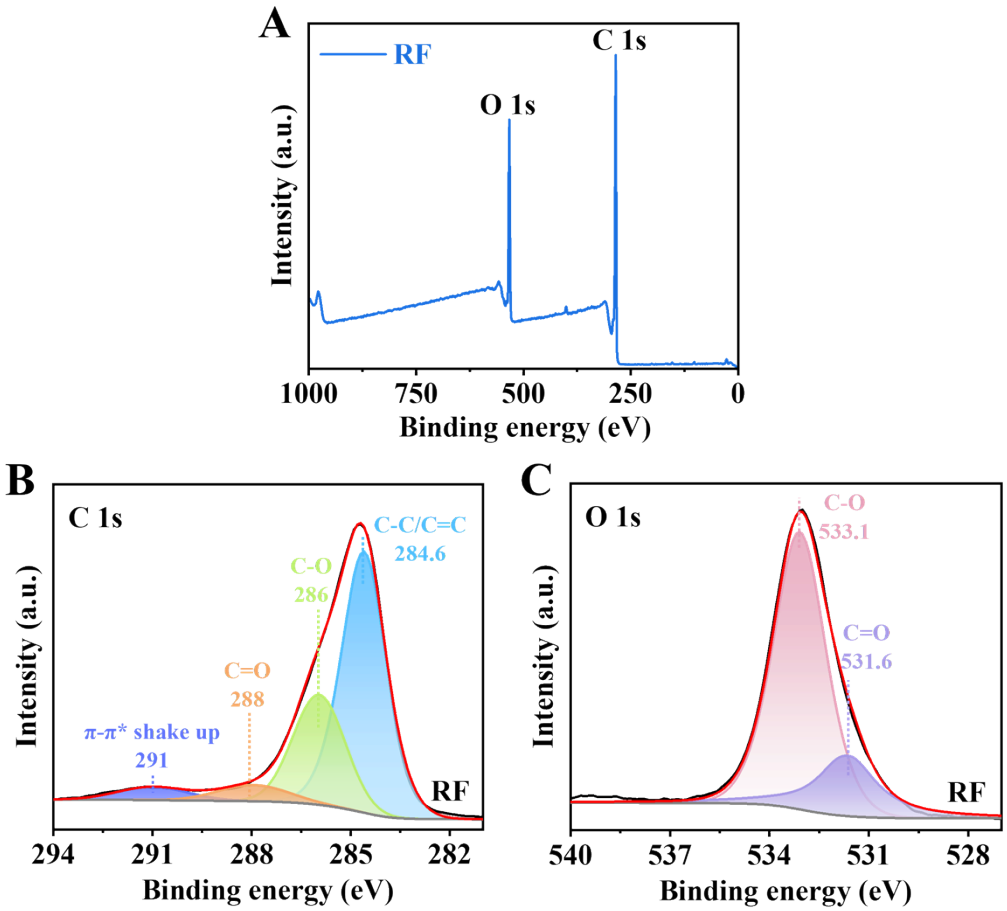

Fig. S6. (A) XPS survey spectra of the RF sample. High-resolution XPS spectra of the RF sample: (B) C 1s and (C) O 1s.

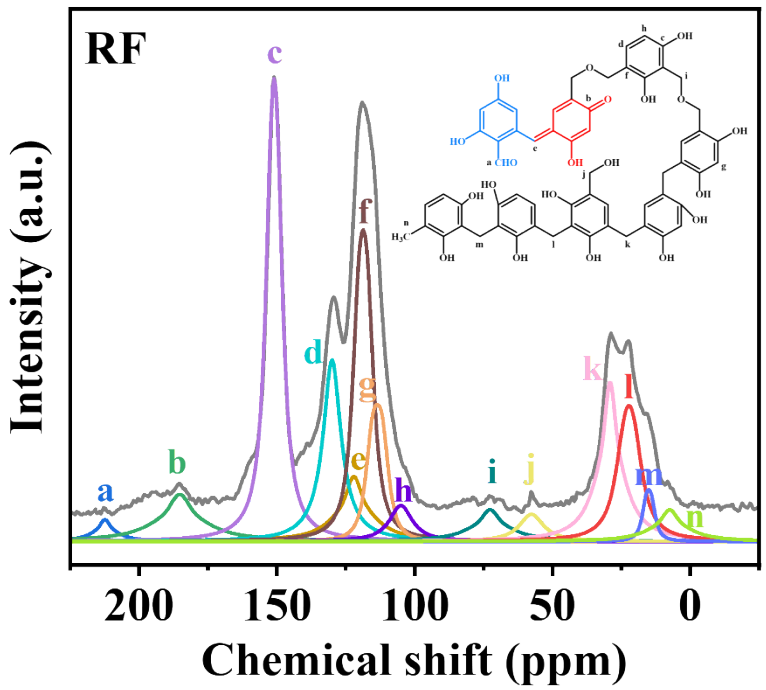

Fig. S7. Solid-state ^{13}C-NMR spectrum of the RF. Assignments of the corresponding carbon components: aldehyde −CHO (213 ppm, *a*), quinone C=O (185 ppm, *b*), resorcinol C−OH (151 ppm, *c*), non-substituted resorcinol C at the *meta* position (130 ppm, *d*), methine linker −C= (122 ppm, *e*), substituted resorcinol C (119 ppm, *f*), non-substituted resorcinol C at the *para* and *ortho* positions (114 ppm, *g*; 105 ppm, *h*), methylene ether linker −C−O−C− (73 ppm, *i*), methylol C−OH (58 ppm, *j*), methylene linker −C− substituted to 4,4′-, 2,4′- and 2,2′-positions of resorcinol (29 ppm, *k*; 22 ppm, *l*; 15 ppm, *m*), and methyl −CH_3 (7 ppm, *n*).

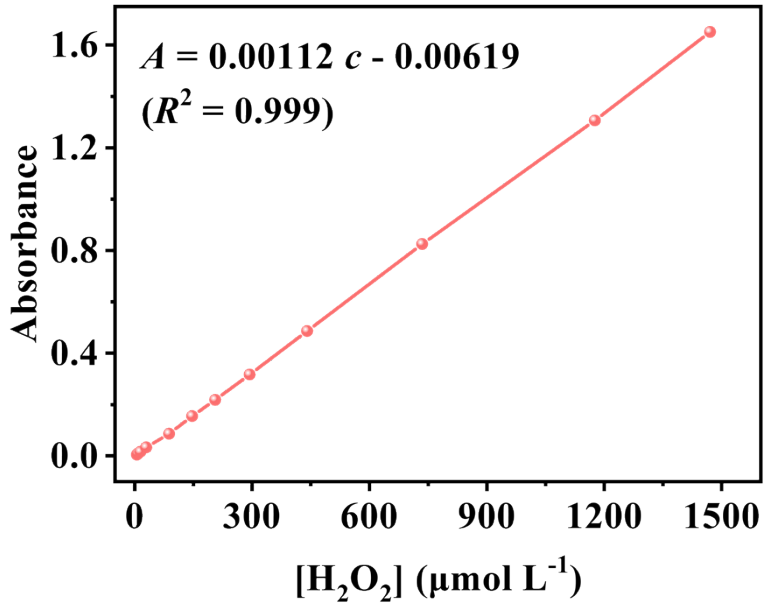

Fig. S8. Linear fitting diagram of the relationship between H_2O_2 concentration and absorbance (λ = 385 nm).

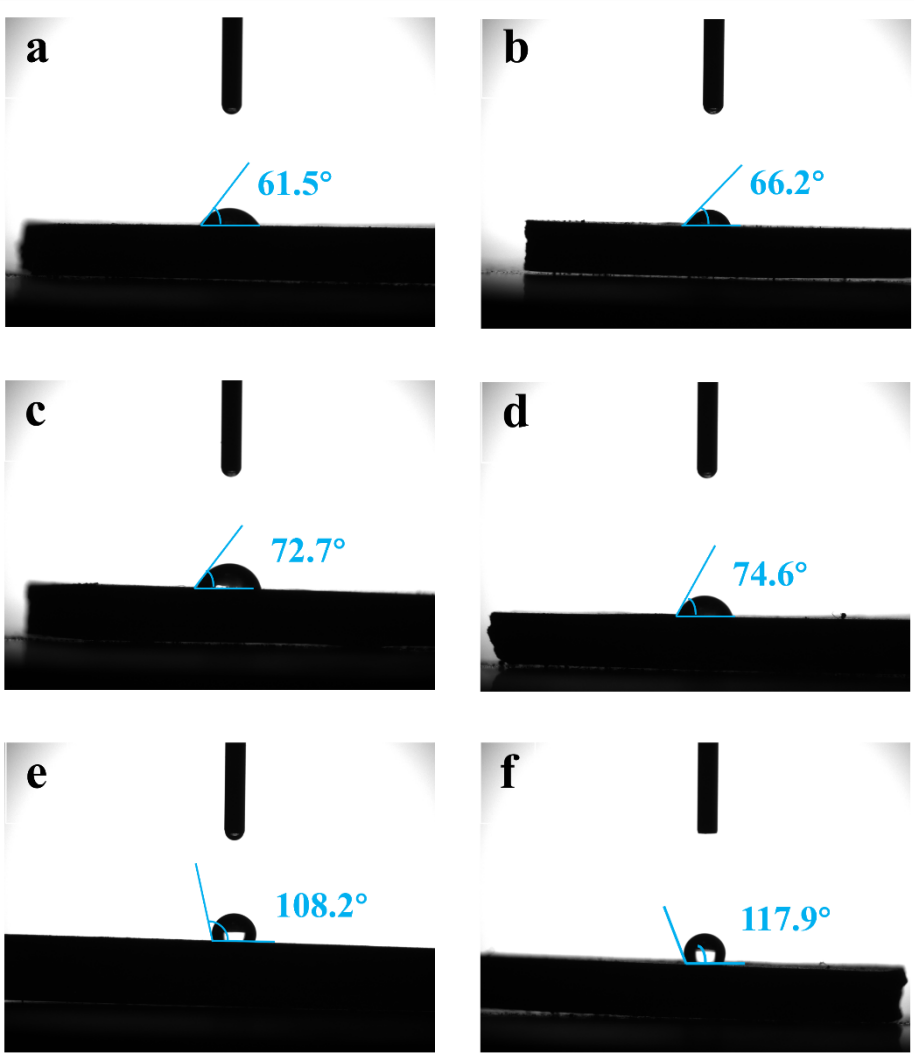

Fig. S9. The measured water contact angles of the (a) RF, (b)T_1RF_{99}, (c) T_3RF_{97}, (d) T_5RF_{95}, (e) T_7RF_{93}, and (f) $T_{10}RF_{90}$ resins.

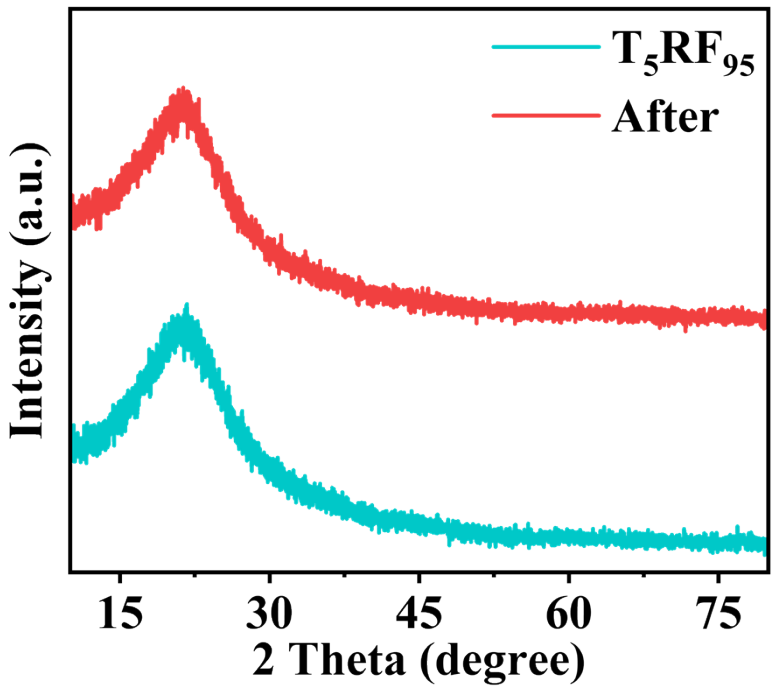

Fig. S10. XRD patterns of the T_5RF_{95} photocatalyst before and after photocatalytic reaction for 2 h.

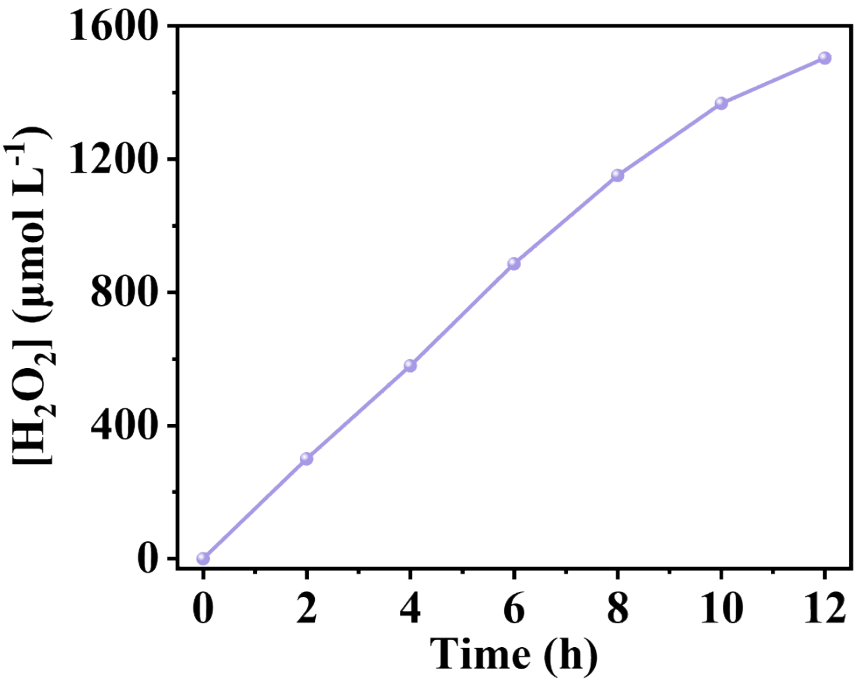

Fig. S11. The long-term stability data of the T_5RF_{95} sample for 12 h. Test condition: pure water (50 mL), catalyst (50 mg), and the O_2 atmosphere.

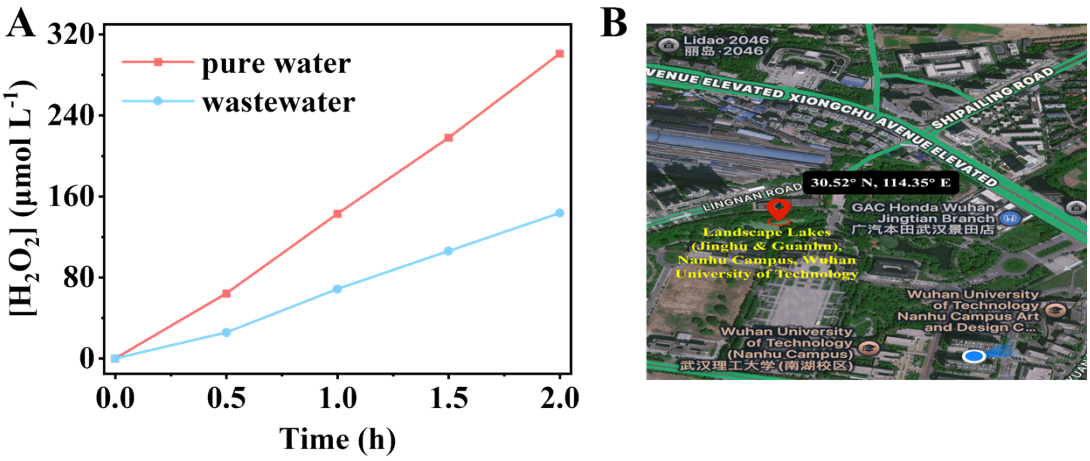

Fig. S12. Photocatalytic H_2O_2 production performance of the T_5RF_{95} sample in different systems. Test condition: wastewater (50 mL), pure water (50 mL), catalyst (50 mg), and the O_2 atmosphere. (B) The location map of sampling site.

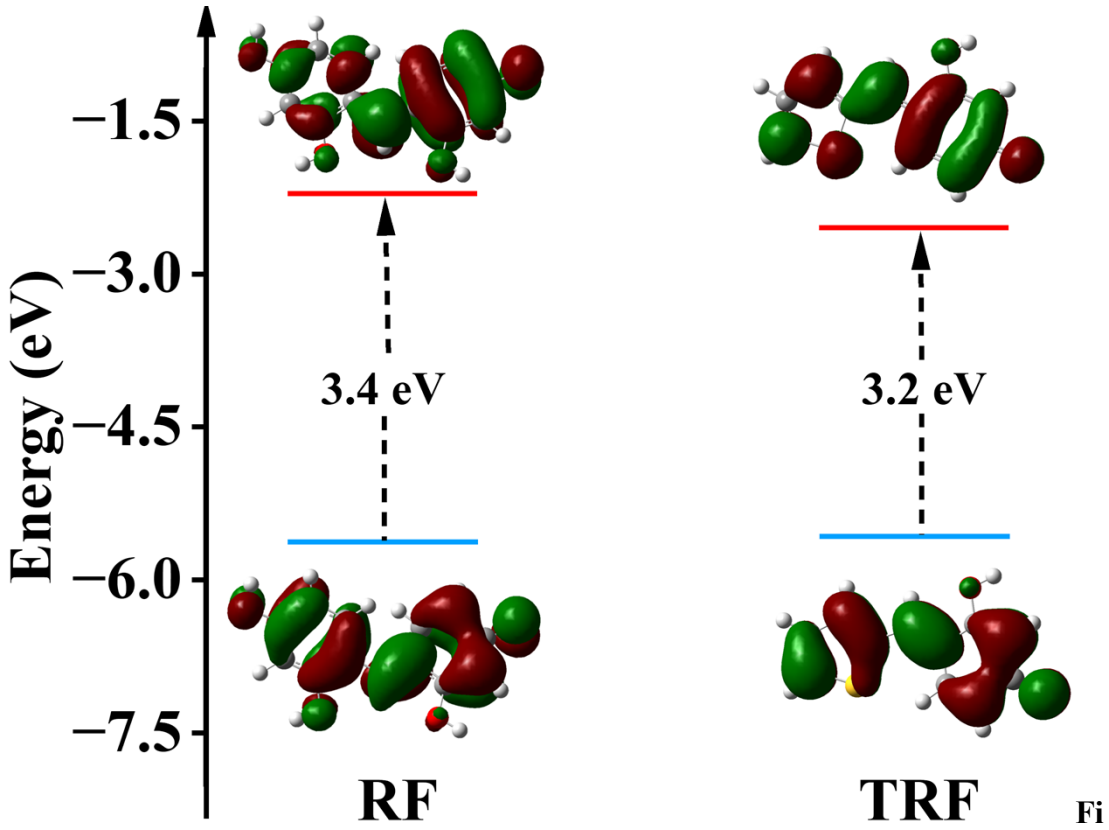

g. S13. Energy diagrams and main molecular orbitals of the RF and TRF.

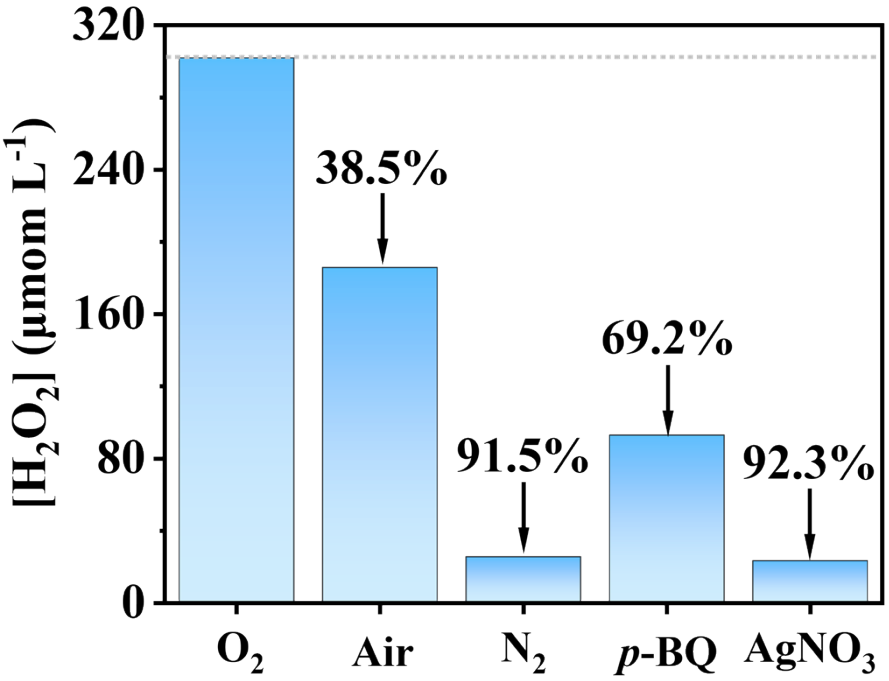

Fig. S14. Photocatalytic H_2O_2 production performance of the T_5RF_{95} resin under different conditions: O_2, Air, N_2, 1 mM *p*-BQ and $AgNO_3$ aqueous solution.

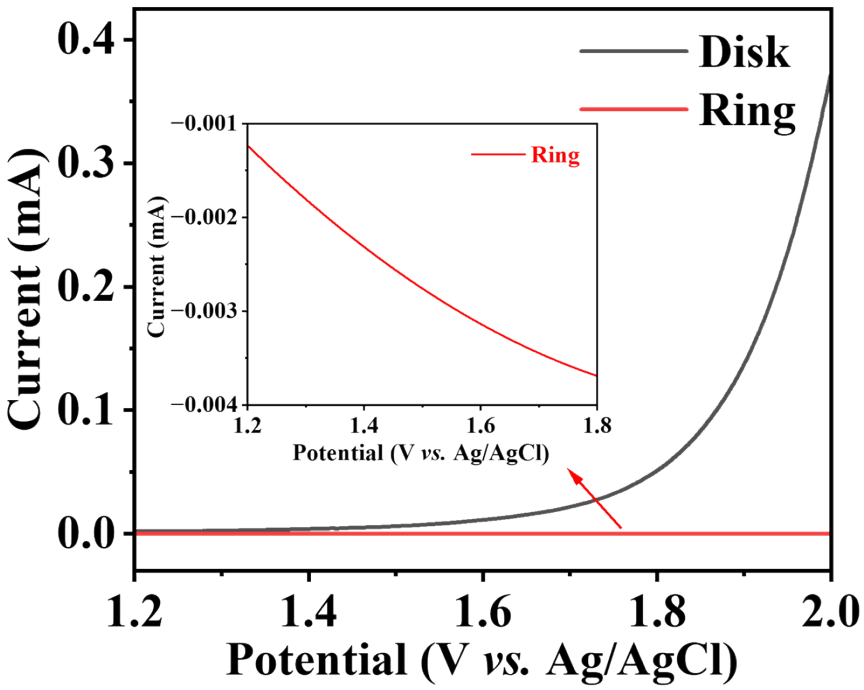

Fig. S15. The RRDE polarization curves in the N_2 atmosphere of the T_5RF_{95} sample. The inset figures show the magnified ring current.

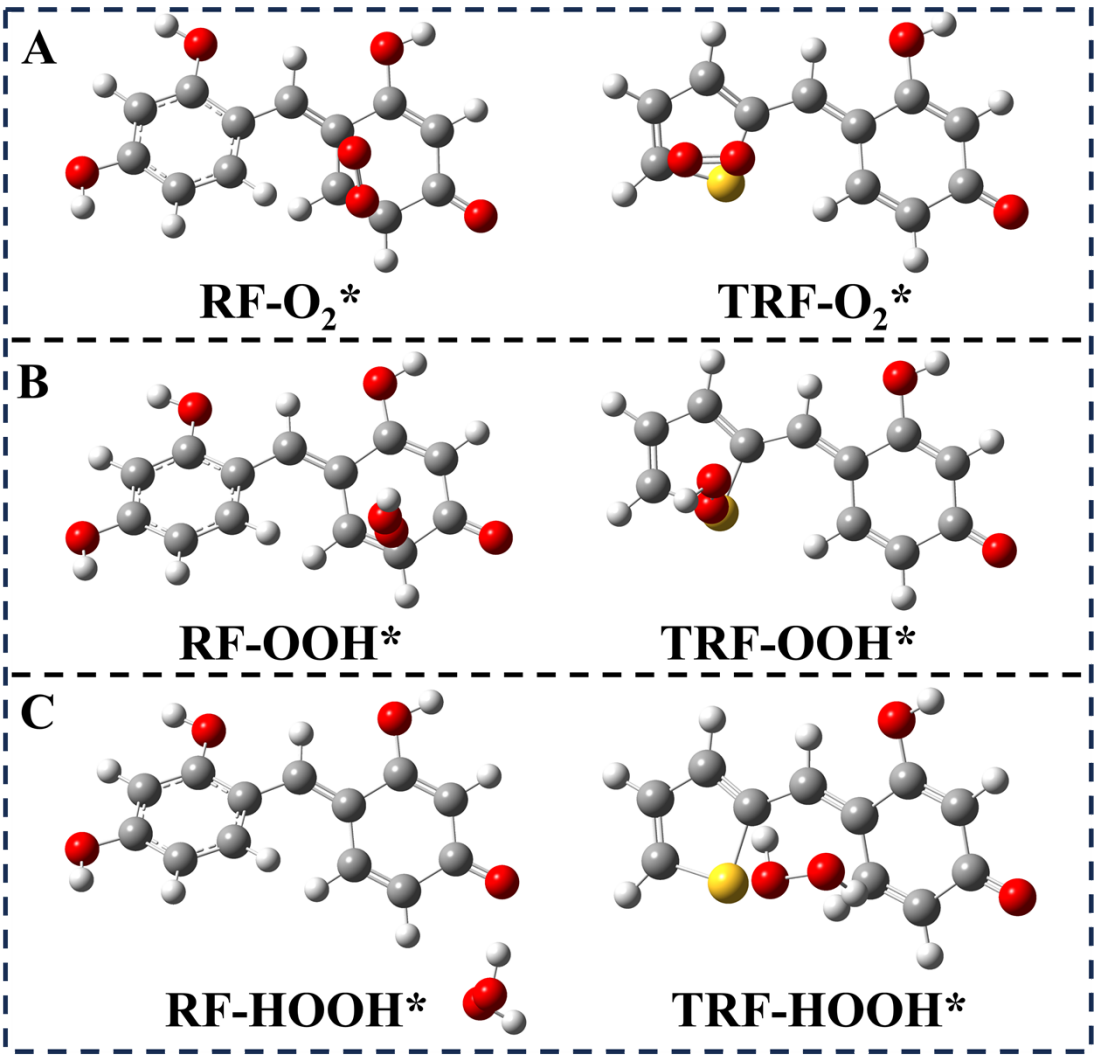

Fig. S16. The theoretical computational models employed for free energy calculations about the oxygen reduction reaction (ORR) process of the RF and TRF.

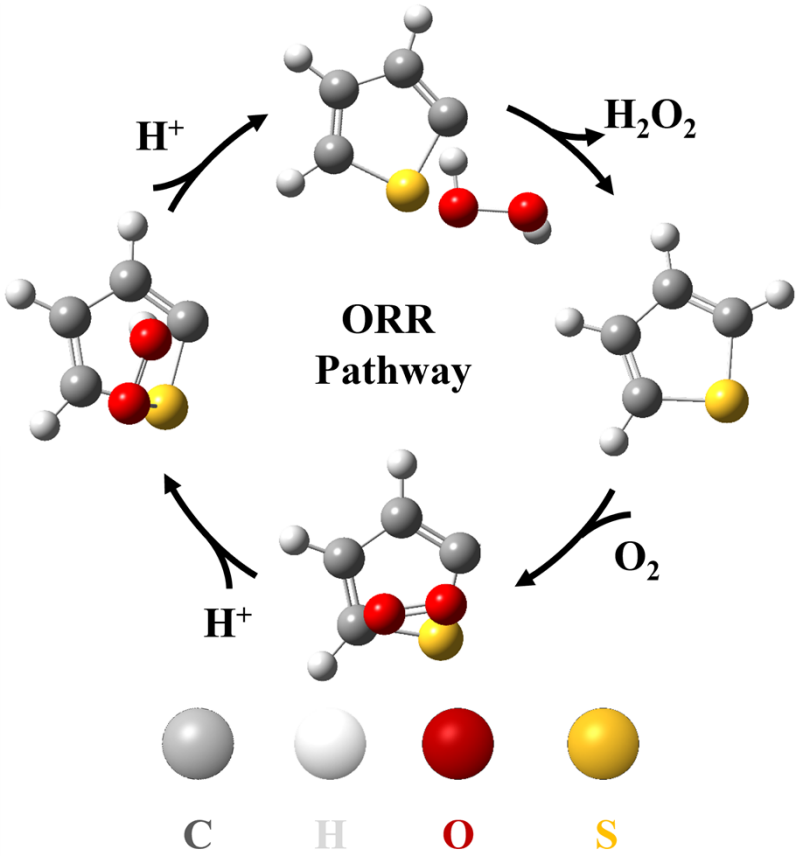

Fig. S17. Schematic diagram of the possible ORR pathway mechanism of the TRF resin.

Supporting Tables

Table S1. The comparison of photocatalytic activity for H_2O_2 production between this work and various reported photocatalysts.

Photocatalysts	Light source	Reaction solution	Activity (μmol L^{-1} h^{-1})	AQY (%)	Ref.
RF523	300 W Xe lamp (λ > 420nm)	Water	86.1	–	7
RF/P3HT-1.0	300 W Xe lamp (λ > 420nm)	Water	390.4	10.5	8
CNOP	300 W Xe lamp (λ > 420nm)	Water, Air	27.5	2.5	9
Nv-C≡N-CN	300 W Xe lamp (λ ≥ 420nm)	Water	137	1.8	10
CTF-BDDBN	300 W Xe lamp (λ > 420nm)	Water	58.3	–	11
NMT400	300 W Xe lamp (AM 1.5G)	Water	108.4	0.5	12
PM-CDs-30	300 W Xe lamp (λ ≥ 420nm)	Seawater, Air	888	0.99	13
TiO_2@RF	300 W Xe lamp (AM 1.5G)	Water	66.7	–	14
RF-BZ	300 W Led lamp (λ > 380nm)	Water	63.83	–	15
F(100)-RF	500 W Led lamp (λ > 380 nm)	Water	272.5	–	16
0.5ZnS@RF-523	3 W LED lamp (420 nm)	Water	73.58	4.66	1
Cu@Au/$BiVO_4$	3 W LED lamp (420 nm)	Water, methanol	31.4	0.88	17
T_5RF_{95}	**3 W LED lamp (420 nm)**	**Water**	**150.9**	**3.04**	**This work**

Table S2. Results of photocatalytic H_2O_2 production on the resins prepared with various thiophene derivatives. [a]

Thiophene derivatives	Structure	$[H_2O_2]$ (μmol L^{-1})[b]
2-thiophene-carboxaldehyde	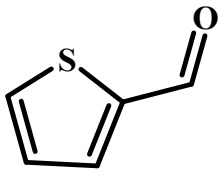	301.8
3-thiophene-carboxaldehyde	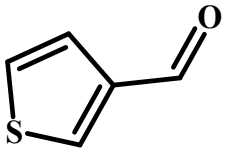	182.1
Thiazole-5-carboxaldehyde	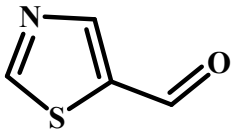	142.9
Benzo[b]thiophene-2-carboxaldehyde	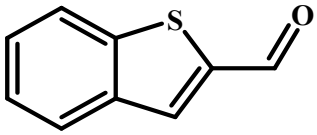	130.4

[a] Synthesis: pure water (60 mL), resorcinol (3.6 mmol), thiophene derivatives (0.36 mmol), formaldehyde (6.84 mmol), ammonia solution (4 mL, 2.8 wt%), hydrothermal treatment (473 K, 24 h).

[b] Reaction conditions: pure water (50 mL), photocatalysts (50 mg), O_2, λ = 420 nm (LED lamp, 12.5 mW cm^{-2}), temperature (298 K), photoirradiation time (2 h).

Table S3. Time-resolved photoluminescence lifetime and relevant percentage data fitted by a three-exponential function.

Photocatalysts	τ_1 (ns)	τ_2 (ns)	τ_3 (ns)	A_1(%)	A_2(%)	A_3(%)	τ_{ave} (ns)
RF	0.5	2.43	9.75	55.04	32.17	12.79	6.16
T_5RF_{95}	0.61	2.86	12.53	55.29	34.2	10.51	7.41
$T_{10}RF_{90}$	0.68	3.03	10.14	35.49	45.18	19.34	6.78

The average lifetime (τ_{ave}) is calculated by the following equation:

$$\tau_{ave} = (A_1\tau_1^2 + A_2\tau_2^2 + A_3\tau_3^2)/(A_1\tau_1 + A_2\tau_2 + A_3\tau_3) \quad \text{(S7)}$$

τ_1, τ_2, and τ_3 correspond to the lifetimes of radiative, non-radiative, and energy transfer processes, and A_1, A_2, and A_3 represent the tri-exponential factors, respectively.

Table S4. The calculated free energies (in the units of eV) for O_2 adsorption at different active sites of the TRF and RF resin.

Computational model	Free energy (eV)
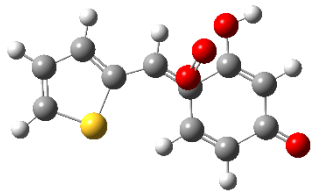	-0.247
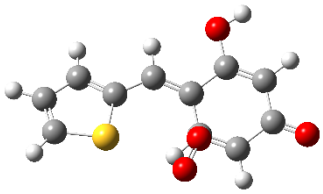	-0.193
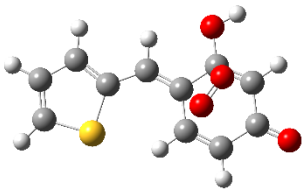	-0.290
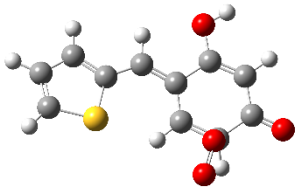	0.073
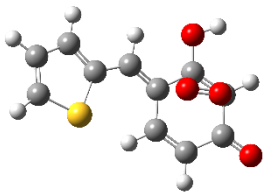	-0.314
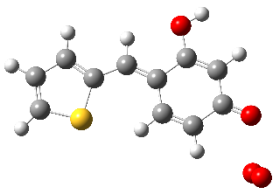	-0.223
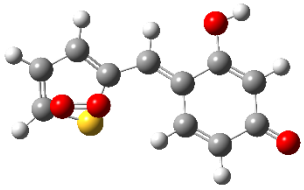	-0.356

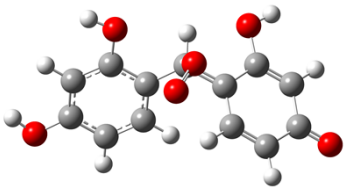	1.481
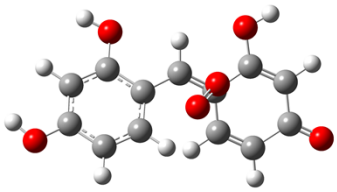	1.393
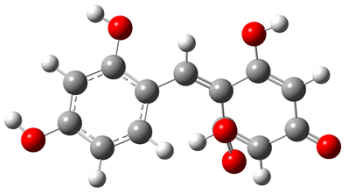	1.355
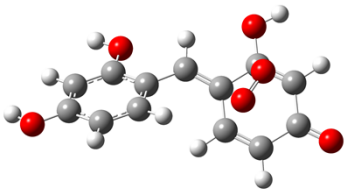	1.377
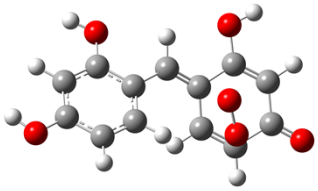	1.353
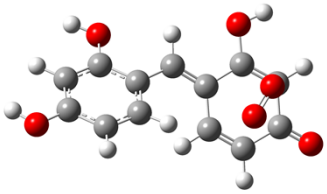	1.371
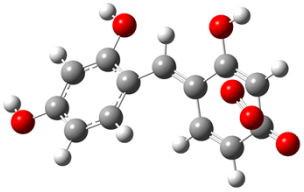	1.461

References

1 Y. Luo, X. Wang, P. Wang, F. Chen and H. Yu, *Chem. Eng. J.*, 2024, **497**, 154886.

2 Z. Chen, C. C. Chu, D. C. Yao, Q. J. Li and S. Mao, *Adv. Funct. Mater.*, 2024, **34**, 9.

3 W. J. Fan, B. Q. Zhang, X. Y. Wang, W. G. Ma, D. Li, Z. L. Wang, M. Dupuis, J. Y. Shi, S. J. Liao and C. Li, *Energy Environ. Sci.*, 2020, **13**, 238-245.

4 X. Wang, X. Yang, C. Zhao, Y. Pi, X. Li, Z. Jia, S. Zhou, J. Zhao, L. Wu and J. Liu, *Angew. Chem. Int. Ed.*, 2023, **62**, e202302829.

5 T. Lu and F. Chen, *J. Comput. Chem.*, 2012, **33**, 580-592.

6 T. Lu, *J. Chem. Phys.*, 2024, **161**, 41.

7 Y. Shiraishi, T. Takii, T. Hagi, S. Mori, Y. Kofuji, Y. Kitagawa, S. Tanaka, S. Ichikawa and T. Hirai, *Nat. Mater.*, 2019, **18**, 985-993.

8 Y. Shiraishi, M. Matsumoto, S. Ichikawa, S. Tanaka and T. Hirai, *J. Am. Chem. Soc.*, 2021, **143**, 12590-12599.

9 H. Kim, K. Shim, K. E. Lee, J. W. Han, Y. F. Zhu and W. Y. Choi, *Appl. Catal. B-Environ. Energy*, 2021, **299**, 9.

10 X. Zhang, P. J. Ma, C. Wang, L. Y. Gan, X. J. Chen, P. Zhang, Y. Wang, H. Li, L. H. Wang, X. Y. Zhou and K. Zheng, *Energy Environ. Sci.*, 2022, **15**, 830-842.

11 L. Chen, L. Wang, Y. Y. Wan, Y. Zhang, Z. M. Qi, X. J. Wu and H. X. Xu, *Adv. Mater.*, 2020, **32**, 10.

12 C. Yang, S. J. Wan, B. C. Zhu, J. G. Yu and S. W. Cao, *Angew. Chem. Int. Ed.*, 2022, **61**, 9.

13 Q. Y. Wu, J. J. Cao, X. Wang, Y. Liu, Y. J. Zhao, H. Wang, Y. Liu, H. Huang, F. Liao, M. W. Shao and Z. H. Kang, *Nat. Commun.*, 2021, **12**, 2.

14 C. H. Xia, L. Yuan, H. Song, C. Q. Zhang, Z. M. Li, Y. Y. Zou, J. X. Li, T. Bao, C. Z. Yu and C. Liu, *Small*, 2023, **19**.

15 X. Y. Li, Q. A. Zheng, X. R. Wang, Q. Y. Zheng, Y. Zhang, Y. Q. Cong and S. W. Lv, *J. Mater. Chem. A*, 2024, **12**, 8420-8428.

16 S. Higashimoto, K. Kishimoto, R. Tokunaga, Y. Harada and T. Kamegawa, *Catal. Today*, 2025, **460**, 7.

17 K. Y. Wang, M. Wang, J. C. Yu, D. Liao, H. Y. Shi, X. F. Wang and H. G. Yu, *ACS Appl. Nano Mater.*, 2021, **4**, 13158-13166.